UCSF

Title

Identification of genetic risk factors in the Chinese population implicates a role of immune system in Alzheimer's disease pathogenesis

Permalink

Journal

ISSN

Authors

Zhou, Xiaopu
Chen, Yu
Mok, Kin Y
et al.

Publication Date

DOI

Peer reviewed

Identification of genetic risk factors in the Chinese population implicates a role of immune system in Alzheimer's disease pathogenesis

Xiaopu Zhou[a,1], Yu Chen[a,b,c,1], Kin Y. Mok[a,d], Qianhua Zhao[e], Keliang Chen[e], Yuewen Chen[a,b,c], John Hardy[d], Yun Li[f,g,h], Amy K. Y. Fu[a,b], Qihao Guo[e,2], Nancy Y. Ip[a,b,2], and for the Alzheimer's Disease Neuroimaging Initiative[3]

[a]Division of Life Science, State Key Laboratory of Molecular Neuroscience and Molecular Neuroscience Center, The Hong Kong University of Science and Technology, Clear Water Bay, Kowloon, Hong Kong, China; [b]Guangdong Provincial Key Laboratory of Brain Science, Disease, and Drug Development, Hong Kong University of Science and Technology Shenzhen Research Institute, Shenzhen, 518057 Guangdong, China; [c]The Brain Cognition and Brain Disease Institute, Shenzhen Institutes of Advanced Technology, Chinese Academy of Sciences, Shenzhen, 518055 Guangdong, China; [d]Department of Molecular Neuroscience, University College London Institute of Neurology, London WC1N 3BG, United Kingdom; [e]Department of Neurology, Huashan Hospital, Fudan University, 200040 Shanghai, China; [f]Department of Genetics, University of North Carolina, Chapel Hill, NC 27599; [g]Department of Biostatistics, University of North Carolina, Chapel Hill, NC 27599; and [h]Department of Computer Science, University of North Carolina, Chapel Hill, NC 27599

Alzheimer's disease (AD) is a leading cause of mortality among the elderly. We performed a whole-genome sequencing study of AD in the Chinese population. In addition to the variants identified in or around the *APOE* locus (sentinel variant rs73052335, $P = 1.44 \times 10^{-14}$), two common variants, *GCH1* (rs72713460, $P = 4.36 \times 10^{-5}$) and *KCNJ15* (rs928771, $P = 3.60 \times 10^{-6}$), were identified and further verified for their possible risk effects for AD in three small non-Asian AD cohorts. Genotype–phenotype analysis showed that *KCNJ15* variant rs928771 affects the onset age of AD, with earlier disease onset in minor allele carriers. In addition, altered expression level of the *KCNJ15* transcript can be observed in the blood of AD subjects. Moreover, the risk variants of *GCH1* and *KCNJ15* are associated with changes in their transcript levels in specific tissues, as well as changes of plasma biomarkers levels in AD subjects. Importantly, network analysis of hippocampus and blood transcriptome datasets suggests that the risk variants in the *APOE*, *GCH1*, and *KCNJ15* loci might exert their functions through their regulatory effects on immune-related pathways. Taking these data together, we identified common variants of *GCH1* and *KCNJ15* in the Chinese population that contribute to AD risk. These variants may exert their functional effects through the immune system.

Alzheimer's disease | whole-genome sequencing | GWAS | risk variant | immune

Alzheimer's disease (AD) is an age-related neurodegenerative disease and a leading cause of mortality in the elderly. Its prevalence is increasing rapidly with the aging population, affecting more than 36 million people worldwide. A recent meta-analysis revealed that the number of AD patients in China increased from 1.9 million in 1990 to 5.7 million in 2010 (1). The pathophysiological mechanisms of AD are complex, with genetic factors playing critical roles. Previous genetics studies, including genome-wide association studies (GWAS), candidate gene sequencing, and whole-exome sequencing have identified several disease genes and risk alleles in AD (2). Among the identified genetic risk factors for AD, a substantial proportion of the genes are associated with immune pathways (3–8).

Most existing genetic data on AD are from Caucasian populations, whereas information for the other ethnic populations is limited. Susceptibility to certain genetic risk factors varies among populations (9). Importantly, even for *APOE-ε4*, the most consistent risk factor for late-onset AD, the risk levels [i.e., odds ratios (ORs)] vary among ethnic groups (10). Furthermore, recent small-scale studies of Chinese populations report that not all of the AD susceptibility SNPs identified in Caucasian populations can be replicated in Chinese AD patients (11). Indeed, variations of the

prevalence of disease-associated genes in different populations have also been observed in other neurodegenerative diseases. For example, the Parkinson's disease susceptibility gene, *MAPT*, a major contributor to the disease in Caucasian populations, is only weakly associated with the disease in the Asian population (12, 13). Similarly, whereas the multiple nonsynonymous variants of *TREM2* are strongly associated with AD in Caucasian populations (3, 4), these associations

Significance

Alzheimer's disease (AD) is an age-related neurodegenerative disease. Genome-wide association studies predominantly focusing on Caucasian populations have identified risk loci and genes associated with AD; the majority of these variants reside in noncoding regions with unclear functions. Here, we report a whole-genome sequencing study for AD in the Chinese population. Other than the *APOE* locus, we identified common variants in *GCH1* and *KCNJ15* that show suggestive associations with AD. For these two risk variants, an association with AD or advanced onset of disease can be observed in non-Asian AD cohorts. An association study of risk variants with expression data revealed their modulatory effects on immune signatures, linking the potential roles of these genes with immune-related pathways during AD pathogenesis.

were not replicated in East Asian populations (14–16). On the other hand, an independent variant in *TREM2* (*p*. H157Y) has been identified as a susceptibility missense mutation for AD in a Chinese cohort (17).

Most genetic risk variants associated with diseases identified from GWAS are located in the noncoding regions, with relatively low disease penetrance. The biological functions of these noncoding variants in diseases such as AD remain largely unknown (18). However, the recent development of genotype–expression analysis can correlate the genotype of AD risk variants with gene transcript level in specific tissues (7); biomarker data, including protein levels (19) or imaging data (20, 21) may provide insights into the roles of these variants in specific biological pathways and predict potential disease risk factors (22). Understanding the effect of these variants in specific cellular contexts enables the study of the functional consequences of these disease-risk genes.

Therefore, it is important to systematically investigate the genetic risk factors for AD in populations of different ethnicities. Furthermore, the successful implementation of genotype–expression analysis for newly identified risk loci may enable us to further investigate the underlying biological mechanism. Our study identified that, in addition to variants in or near the *APOE* locus, two loci—*GCH1* and *KCNJ15*—are associated with AD. Furthermore, the genotype–expression analyses reveal that these AD risk loci are associated with the regulation of immune-related gene networks in the hippocampus and blood, as well as the changes in plasma biomarkers. These findings implicate a role of immune-related pathways in the disease.

Materials and Methods

Subject Recruitment for the In-House Chinese AD Whole-Genome Sequencing Cohort. For this study, we included a cohort of Chinese subjects who visited the Department of Neurology or Memory Clinic, Huashan Hospital, Fudan University, Shanghai, China from 2007 to 2016. There were a total of 972 subjects including 489 with AD, 260 with mild cognitive impairment (MCI), and 223 age- and gender-matched normal controls (NCs). AD patients were diagnosed on the basis of the recommendations of the National Institute on Aging and the Alzheimer's Association workgroup (23) and had an onset age ≥50 y. Patients with MCI were diagnosed according to the Peterson criteria (24). We excluded individuals with any significant neurologic disease or psychiatric disorder. In addition, 250 NCs without subjective memory complaints were recruited from the community in Shanghai. We subjected all subjects to medical history assessment, neuropsychological assessment, and imaging assessment including computed tomography (CT) or magnetic resonance imaging (MRI). Some subjects also underwent positron emission tomography using Pittsburgh compound B. This study was approved by the Ethics Committee of Huashan Hospital, the Hong Kong University of Science and Technology (HKUST), and the HKUST Shenzhen Research Institute. All subjects provided written informed consent for both study enrollment and sample collection.

CONVERGE Chinese Whole-Genome Sequencing Cohort. We included the CONVERGE (China Oxford and Virginia Commonwealth University Experimental Research on Genetic Epidemiology) whole-genome sequencing (WGS) dataset (*n* = 10,640) to serve as a multicenter control to generalize the results (25). We applied an age filter of ≥55 y for the elderly population, yielding 1,745 subjects (*n* = 1,745) for the downstream analysis.

WGS and Variant Calling Method. Low-coverage WGS (5× coverage) was performed by Novogene. The genomic DNA libraries were sequenced on an Illumina Hiseq × Ten platform, with 150-bp paired-end reads generated. The researchers were blinded to phenotypic labels during the WGS process. For variant detection, the Gotcloud pipeline (26) was adopted to detect variants from our low-pass WGS data, comprising 1,348 samples, including 126 resequenced samples. An average of 15-Gb Illumina sequencing data per subject were generated, and data were subsequently subjected to *FastQC* (27) for quality checking and *Trimmomatic* (28) for the trimming and filtering of low-quality reads. Clean data were mapped to the GRCh37 reference genome containing the decoy fragments using *BWA-mem*. After de-duplication and clipping of the overlapped paired-end reads, BAM files were subjected to *samtools-hybrid*, a specialized version of *samtools*, to generate glf files, which store the marginal likelihoods for genotypes. glfFlex was adopted for the

population-based SNP calling, with a total of 24,742,555 single-nucleotide variants obtained after variant calling. We applied hard-filtering methods implemented in the Gotcloud pipeline as VcfCooker to filter low-confidant variant calls on the basis of multiple metrics, such as distance, with known insertion/deletion sites, allele balance, and mapping quality. We subjected variants with high-confidence calls in the range of minor allele frequency (MAF) ≥ 5% (*n* = 5,523,365; 22.3% of raw detected sites, 5,369,369 of which were in autosomal chromosomes) to Beagle (29, 30) for phasing and using the genotype likelihood information in chromosome-separated VCF files (See *SI Appendix, SI Materials and Methods* for details).

To assess the accuracy of variant detection, we resequenced 126 of 1,222 samples (10.3% of all samples) using the same WGS protocol, together with 96 samples (7.9% of total samples) genotyped using the Axiom Genome-Wide CHB 1 and CHB 2 Array Plate Set (Affymetrix). See *SI Appendix, SI Materials and Methods* for additional details.

Association Test and Data Visualization for GWAS. We performed association tests between cases and controls using PLINK software with the following parameters: –*keep-allele-order*, –*assoc*, –*ci 0.95*, –*hwe 0.00001*, and –*maf 0.10* for the stage 1, stage 2, and stage 1+2 analyses. A genomic inflation factor was generated on the basis of the χ^2-values obtained from PLINK results using R programming (31). In addition, to correct for population stratification, we performed conditional logistical regression combined with a genetic similarity score matching (GSM) model (32) or logistic regression combined with phenotype-associated principal components generated from EIGENSOFT *smartpca* (33). For GSM correction, pruned SNP sets with an MAF > 10% were subjected to the software *score_match* (Linux) (-*s alleleibs -k 2 -m 10000 -model additive -w 10 -U 5 -Ut 5*), with matched results further subjected to R for conditional regression test using *clogit* function. To visualize the data, Manhattan plots and quantile–quantile plots were generated using the R *qqman* package. Regional plots for individual loci were generated using LocusZoom (34). To generate regional plots, association test results were obtained from PLINK, with pairwise linkage disequilibrium (LD) information generated from VCFtools using the –*hap-r2* option.

Cohorts and Data for Replication Study. To verify our findings, we obtained the following data: (*i*) The International Genomics of Alzheimer's Project (IGAP) summary statistics from stage 1 data (35); (*ii*) genotype, transcriptome, and biomarker data from the Alzheimer's Disease Neuroimaging Initiative (ADNI) database (adni.loni.usc.edu/) (36); (*iii*) genotype and phenotype data from the National Institute on Aging Alzheimer's Disease Centers Cohort (ADC) (phs000372.v2.p1) (37); and (*iv*) genotype and phenotype data from the Late Onset Alzheimer's Disease (LOAD) Family Study (phs000168.v2.p2) (38). See *SI Appendix, SI Materials and Methods* for additional details.

Meta-Analysis and Data Visualization. We generated association results from three AD cohorts (ADNI, LOAD, and ADC) using logistic regression with phenotype-associated principal components generated from EIGENSOFT *smartpca*, together with age and gender as covariates to obtain effect sizes (log-ORs) and SEs. The analysis only included "definite AD" cases which were specified in ADC and LOAD cohorts. The results were summarized and processed by METASOFT (39) to estimate the joint risk effects as well as significance levels under a random effects (RE) model (meta-*P* value or random-effect *P* value). For transethnic meta-analysis combining both Chinese and non-Asian datasets, Han and Eskin's Random Effects model (39) was applied. Analysis results were further subjected to ForestPMPlot (40) to generate forest plots for data visualization.

Association Analysis for Candidate Sites in Transcriptome Data and in Plasma and Cerebrospinal Fluid Biomarker Data. We retrieved genotype and expression data from the Genotype-Tissue Expression (GTEx) project (41, 42) (www.gtexportal.org) in the database of Genotypes and Phenotypes (dbGaP; phs000424.v6.p1). We used the R *GenABEL* package (43) for data normalization, then mapped the regulatory effects of our candidate variants using R coding and generated network analysis of the top regulatory genes in STRINGdb (44). We examined the association of the candidate variants with the plasma and cerebrospinal fluid biomarker data obtained from the ADNI (*SI Appendix, SI Materials and Methods*).

Other Statistical Analyses and Data Visualization. We performed Cox regression with gender and the top five principal components (PCs) to determine the association between AD onset age and candidate variants by using the *coxph* function from the *survival* package in R. We performed the Spearman correlation test using the *cor.test* function in R. We used *ggsurvplot* from the *survMisc* package to generate the survival plot. We

generated bar charts, scatter plots, and line charts by using GraphPad Prism version 6 (GraphPad software) (45). We used R *lm* function together with *Anova* function from *car* package for ANCOVA analysis. Finally, we obtained gene annotations from database evidence, with annotations for genomic regions obtained from the University of California, Santa Cruz genome browser (46) and annotations for transcript enrichment from the FANTOM CAT data browser (47).

Power Calculation. According to the study design for the stage 1 analysis (NC: 442; AD: 477), power calculation was performed using Quanto (48). The prevalence of AD was set at 3.3% on the basis of the latest epidemiological report for AD in the Chinese population (5.5 million AD patients of 165.2 million subjects with age ≥60-y old; data were obtained from summary results in 2010 with age ranging between 60 and 99 y) (1). The following parameters were applied: outcome, disease; design, unmatched case–control (1:0.9266); hypothesis, gene only; sample size, 477 cases; significance, 1×10^{-4}, two-sided; mode of inheritance, log-additive; population risk, 0.033.

Data Availability. The summary-level statistics for the reported variants (59 sites) are available at: iplabdatabase.ust.hk/zhou_et_al_2017/GWAS_data.html. A file containing allele frequencies for variants analyzed in this paper (MAF ≥ 10%) is available through application via the above URL.

Results

Identification of AD Susceptibility Loci in the Chinese Population. We recruited a Chinese AD cohort comprising 1,222 participants and subjected them to low-pass WGS (5× coverage) (Fig. 1 and *SI Appendix*, Table S1) (49). Our WGS data yielded 5,369,369 autosomal variants with an MAF ≥ 5%. Genotyping quality was assessed by replicating the WGS with duplicate samples ($n = 126$), array genotyping ($n = 96$), and genotyping of *APOE*-ε4 variants (rs429358 and rs7412) ($n = 1,172$) using independent aliquots of genomic DNA; overall genotype concordance rates were 0.982, 0.991, and 0.980, respectively (*SI Appendix*, Tables S2–S4; see also *Materials and Methods* and *SI Appendix, SI Materials and Methods*). After 50 subjects were excluded during the quality-control steps (*Materials and Methods* and *SI Appendix, SI Materials and Methods*), the study population consisted of 477 AD subjects (AD group, $n = 477$), 253 with MCI (MCI group, $n = 253$), and 442 corresponding age- and gender-matched NC subjects (NC group, $n = 442$). All of the analyzed subjects were from the same center and had a similar demographic background. A detailed analysis of ethnic attributes by comparing the WGS data with 1000 Genomes phase 3 data (www.internationalgenome.org/data) demonstrated that our cohort is part of the East Asian ethnic group (*SI Appendix*, Figs. S1 and S2).

The statistical power of our in-house dataset for the identification of AD risk variants with an odds ratio of 1.8 was 0.6073 for an MAF of 0.10, and 0.2078 for an MAF of 0.05 (*Materials and Methods*). Thus, a variant pool containing 4,082,229 sites with an MAF ≥ 10% after filtering low-quality calls was retained for the analysis of our in-house WGS data (stage 1), with a total of 403 variants showing nominal $P < 1 \times 10^{-4}$. To further increase sample size, enhance statistical power, and verify the findings from stage 1, we conducted the stage 2 analysis separately by using the same AD samples from stage 1 ($n = 477$) with the CONVERGE samples ($n = 1,745$, treated as population controls in contrast to the age- and gender-matched cognitive normal controls in stage 1) (*Materials and Methods* and *SI Appendix*) in the stage 2 analysis (25). Of 403 sites, we successfully detected 377 concordant sites in the CONVERGE dataset and 92 biallelic variants surviving from the same nominal P value threshold of 1×10^{-4}.

After controlling for the concordance of both allele orders (i.e., ensuring minor alleles are consistent in the two stages) and direction of effect [i.e., log(OR) has the same sign in both stages], we applied a nominal P value threshold of 5×10^{-8} as the final selection criteria in the combined analysis using all samples (477 AD cases and 442 age- and gender-matched cognitive normal controls from stage 1, with 1,745 population controls from CONVERGE) to further enhance power (stages 1+2). Furthermore, we removed one locus with an MAF that deviated
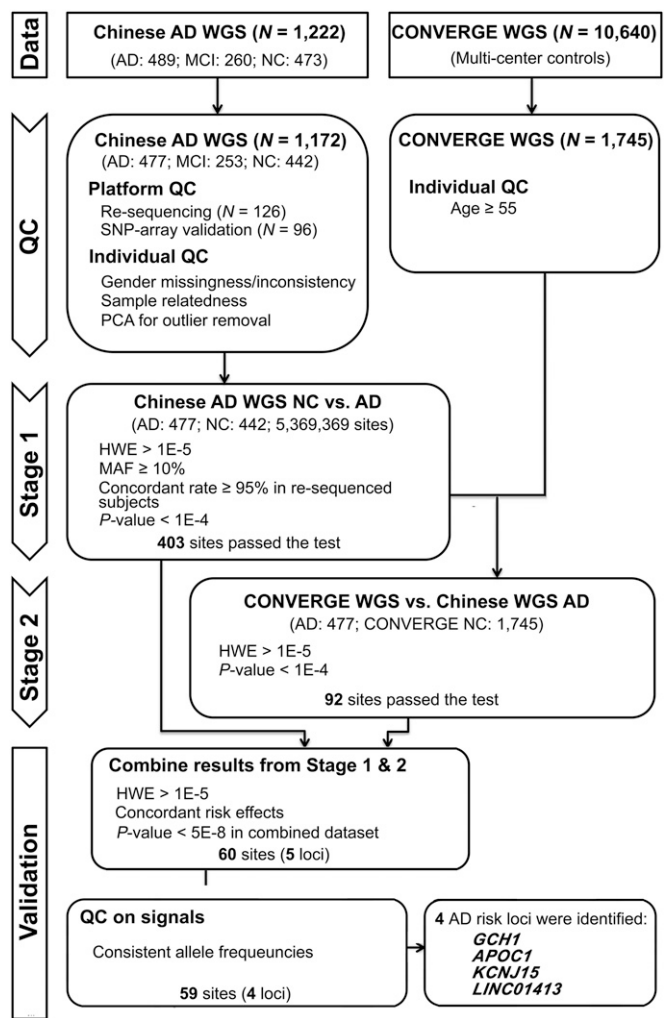

Fig. 1. Study design schematic for the discovery of AD susceptibility loci. HWE, Hardy–Weinberg equilibrium; PCA, principal-component analysis; QC, quality control.

strongly in the in-house NC and CONVERGE dataset. Finally, we obtained 59 variants located in the four loci that passed the threshold: *APOE*, *GCH1*, *LINC01413*, and *KCNJ15*. Other than confirmation of the well-studied *APOE*-ε4 variant rs429358 ($P = 4.1 \times 10^{-64}$), the four sentinel variants were as follows: *GCH1*: rs72713460, $P = 4.0 \times 10^{-8}$, OR = 1.74 (95% CI: 1.42–2.12); *LINC01413*: rs2591054, $P = 3.5 \times 10^{-10}$, OR = 0.61 (95% CI: 0.53–0.71); *APOC1*: rs73052335, $P = 3.5 \times 10^{-72}$, OR = 4.27 (95% CI: 3.61–5.05); and *KCNJ15*: rs928771, $P = 1.2 \times 10^{-8}$, OR = 1.59 (95% CI: 1.38–1.93) (Fig. 2*A*, Table 1, and *SI Appendix*, Table S5). Besides the *APOE*-ε4 variant rs429358, the analysis revealed multiple variants including the sentinel variant rs73052335 near the *APOE* locus (*SI Appendix*, Table S5). The variant rs73052335 was in LD ($R^2 = 0.70$) with *APOE*-ε4 rs429358 (Fig. 2*B*). Regarding the AD susceptibility variants identified in the stage 1 analysis (i.e., *APOC1* rs12721046, *SAMD4A-GCH1* rs17737822, *KCNJ15* rs928771, and *LINC01413* rs2591054), the combined analysis, which merged the controls from the stage 1 and 2 datasets, further boosted the signals of these loci (Fig. 2 *B–D* and *SI Appendix*, Table S5). Specifically, the sentinel variants for the *APOC1* locus shifted from rs12721046 to rs73052335, while the sentinel variants for the *GCH1* locus shifted from rs17737822 to rs72713460 (Fig. 2 *B* and *C*). Notably, we did not observe any inflation during the stage 1

Fig. 2. GWAS results in the Chinese AD WGS study. (*A*) Manhattan plots showing AD susceptibility loci discovered in the Chinese AD WGS dataset. Horizontal lines represent the suggestive threshold ($P = 1E-5$, blue) and genome-wide threshold ($P = 5E-8$, red). The 59 sites that survived the genome-wide threshold in the validation stage are shown as enlarged red dots, with gene symbols marked in the plot. (*B–D*) Regional association plots of the *APOC1* (*B*), *GCH1* (*C*), and *KCNJ15* (*D*) loci. Horizontal lines separate the association results from the stage 1 and stage 1+2 analyses. Purple diamonds specify the sentinel variant in the corresponding locus. Colors illustrate the LD measured as R^2 between the sentinel variant and its neighboring variants. cMMb, centimorgans per megabase.

analysis, as indicated by the quantile–quantile plot and the estimated genomic inflation factor ($\lambda_{GC} = 1.011$, $\lambda_{1000} = 1.025$) (*SI Appendix*, Fig. S3). Moreover, we showed that the presence of effect alleles from the newly identified loci (*GCH1*, *LINC01413*, and *KCNJ15*) were not correlated with age, gender, or batch effects in the combined control datasets (*SI Appendix*, Tables S6 and S7), and was not obviously affected by population stratification after correction using the GSM method (*GCH1*: rs72713460, adjusted $P = 2.5 \times 10^{-7}$; *LINC01413*: rs2591054, adjusted $P = 3.7 \times 10^{-10}$; *KCNJ15*: rs928771, adjusted $P = 3.2 \times 10^{-8}$) (*SI Appendix*, Table S8) (32). While in the stage 1+2 data, among the top 20

PCs, only the first and third were significantly associated with AD (at nominal level P value threshold of < 0.05). Therefore, we selected phenotype-associated PCs together with age and gender as covariates to adjust for possible population stratification and batch effects (50). Although the overall significance level decreased after covariate adjustment, our candidates still reached the suggestive association threshold ($P < 5 \times 10^{-5}$) (*GCH1*: rs72713460, adjusted $P = 4.36 \times 10^{-5}$; *LINC01413*: rs2591054, adjusted $P = 3.65 \times 10^{-5}$; *KCNJ15*: rs928771, adjusted $P = 3.60 \times 10^{-6}$), implying their associations with AD in Chinese population (Table 1 and *SI Appendix*, Tables S8 and S9).

Table 1. GWAS results of AD susceptibility loci discovered in the Chinese AD cohort

					EAF (NC)		Nominal *P* value		Final association results (adjusted results)	
CHR:BP (GRCh37)	SNP_ID	Nearest Gene(s)	EA	EAF (AD)	Stage 1	Stage 1+2	Stage 1	Stage 1+2	Adjusted *P* value	Effect size (SE)
14:55297043	rs72713460	GCH1	T	0.160	0.097	0.099	5.9E−05	4.0E−08	4.36E−05	0.594 (0.145)
15:57612410	rs2591054	LINC01413	C	0.683	0.773	0.779	1.8E−05	3.5E−10	3.65E−05	−0.447 (0.108)
19:45420082	rs73052335	APOC1	C	0.325	0.153	0.101	7.1E−18	3.5E−72	1.44E−14	0.870 (0.113)
21:39663760	rs928771	KCNJ15	G	0.238	0.154	0.161	6.0E−06	1.2E−08	3.60E−06	0.555 (0.120)

Statistical results of four sentinel variants (i.e., variants with the lowest nominal P values among four AD susceptibly loci from the validation stage). Stage 1 (AD: 477, NC: 442); Stage 1+2 (AD: 477, NC: 2,187). BP, base positions in GRCh37 annotation; CHR, chromosome(s); EA, effect alleles; EAF, effect allele frequency.

Replication Study in Non-Asian AD Cohorts. To justify our finding for the AD risk factors, we first examined the summary metrics from the IGAP stage 1 study (sample size $n = 17,008$ and $37,154$, for AD and NC, respectively) (35). Of the three identified variants, none have been reported to be significantly associated with AD ($P = 0.225$, 0.793, and 0.349 for *GCH1* rs72713460, *LINC01413* rs2591054, and *KCNJ15* rs928771, respectively). Meanwhile, a concordant sign of β (i.e., effect size) was observed for *KCNJ15* and *GCH1* variants, implying a possible enrichment of risk alleles of identified risk variants in the non-Asian AD subjects [β = 0.594 (rs72713460-T) and 0.555 (rs928771-G) in the present Chinese study; β = 0.025 (rs72713460-T) and 0.014 (rs928771-G) in the IGAP dataset].

Because the IGAP study included a proportion of AD cases registered as "probable" or "possible" cases (35), we attempted to verify our findings using a subset of cohorts from the IGAP study (i.e., ADNI, ADC, and LOAD) by only retaining the subjects categorized as "definite AD" as cases. Subsequent meta-analysis to summarize the association results of the three sentinel AD risk variants confirmed the AD risk effects of *GCH1* rs72713460 in the non-Asian populations (meta-$P = 1.55 \times 10^{-2}$, OR = 1.109) (Fig. 3A and Table 2). Moreover, we observed a concordant trend of the possible risk effect for the G allele of *KCNJ15* rs928771 among the three datasets, although this failed to pass the significance threshold in the meta-analysis (meta-$P = 1.19 \times 10^{-1}$) (Fig. 3B and Table 2). Although a concordant risk effect was observed for *LINC01413* variant rs2591054 in one of the non-Asian AD cohorts

(ADC, $P = 8.27 \times 10^{-3}$, OR = 0.963) (Table 2 and *SI Appendix,* Fig. S4), an inconsistent risk effect was observed in other cohorts. Therefore, additional genetic evidence is required to validate the association between *LINC01413* and AD.

Additional transethnic meta-analysis summarizing the results from both the Chinese and non-Asian cohorts showed that our candidates exhibited trends of associations with AD in the meta-analysis (*GCH1*: rs72713460: meta-$P = 2.53 \times 10^{-4}$; *KCNJ15*: rs928771, meta-$P = 6.41 \times 10^{-4}$) (Table 2 and *SI Appendix,* Table S10). The results also showed heterogeneity across the Chinese and non-Asian populations, as indicated by the shifting of values in the heterogeneity measurements (I^2 and Cochran's Q-values) (Table 2 and *SI Appendix,* Table S10).

Interestingly, although the meta-analysis failed to replicate the risk effects of *KCNJ15* rs928771, using the definite AD cases in the LOAD dataset, we showed that *KCNJ15* rs928771 exerts an effect on the age of onset in AD. The minor allele G of variant rs928771 was associated with the onset age of AD with a hazard ratio (HR) of 1.197 ($P = 0.0057$, Cox regression model) (Fig. 3C); that is, AD subjects harboring two copies of the minor allele exhibit an earlier disease onset age compared with subjects with homozygous reference alleles (average onset age of AD: 73.4 and 71.2 y for rs928771 genotypes TT and GG, respectively) (Fig. 3D). This finding further suggests a link between *KCNJ15* risk variants or gene with AD pathogenesis.

Functional Implications of Identified Risk Loci from Transcriptome and Biomarker Data. For the *KCNJ15* AD risk locus, we found that *KCNJ15* transcript level was enriched in blood samples ($P = 6.33 \times 10^{-7}$, fold-enrichment: 10.6) (Fig. 4A), implying that this gene plays roles in the peripheral circulatory system. Genotype and phenotype association analysis of *KCNJ15* transcript level in the whole-blood transcriptome dataset revealed that the transcript level was significantly higher in the blood of the AD group than the NC group (Fig. 4B, *Left*). Nonetheless, the sentinel AD risk variant of *KCNJ15*, rs928771, was strongly associated with a decrease of *KCNJ15* transcript level in both the NC and AD groups (Fig. 4B, *Right*). Interaction analysis in NC and AD subjects using a linear regression model indicated a hint of a negative interaction effect (effect size = −0.1278, $P = 0.1601$) between the presence of AD and the rs928771 G allele dosages for *KCNJ15* transcript levels (*SI Appendix,* Fig. S5A). More specifically, a strong association of *KCNJ15* transcript level and rs928771 G allele dosage was also observed in the MCI subjects (effect size = −0.2890, $P = 3.83 \times 10^{-5}$) (*SI Appendix,* Fig. S5B), and a positive correlation between *KCNJ15* transcript level and cognitive performance (indicated by Mini-Mental State Examination score) was observed in the AD cases (effect size = 1.6318, $P = 0.0294$) (*SI Appendix,* Fig. S5C). These results suggest that intrinsic factors, specifically genomic variations, as well as extrinsic factors, specifically disease context, contribute to the regulation of *KCNJ15* gene expression in blood.

To further investigate the potential contributions of variant rs928771 in AD subjects for blood-related traits, we examined the association of AD patients' plasma biomarker levels with rs928771 genotypes. Interestingly, AD subjects showed genotype-dependent reductions of various immune-associated plasma biomarkers, including decreased TNF-related apoptosis-inducing ligand receptor 3 (TRAILR3), metallopeptidase inhibitor 1 (TIMP-1), and α-1-microglobulin (A1M) (Fig. 4C). Further inclusion of control subjects confirmed the effect of the *KCNJ15* variant in the modulation of serum TRAILR3 levels, as evidenced by the concordant reduction of TRAILR3 level in AD and NC subjects harboring rs928771 risk alleles. Moreover, for TIMP-1 and A1M, they both exhibited phenotype-dependent elevation of protein levels in AD subjects, implying their possible roles in AD progression, which may be associated with *KCNJ15* regulations (Fig. 4C and *SI Appendix,* Tables S11 and S12).
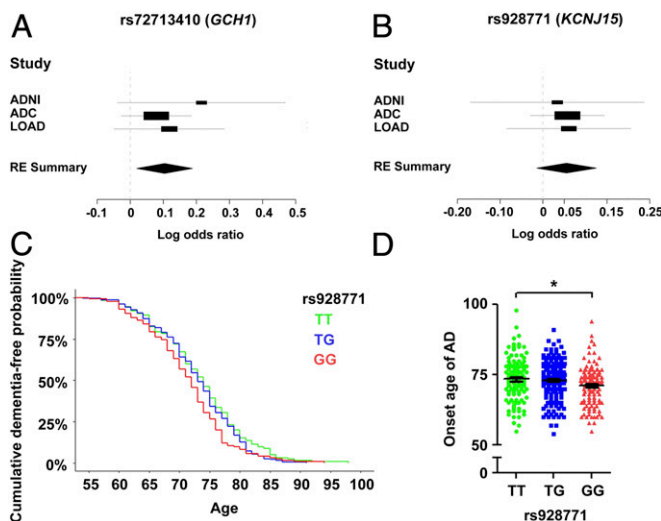

Fig. 3. Replication study in non-Asian AD cohorts. (A and B) Forest plots representing the meta-analysis results of rs72713460 (*GCH1*; A) and rs928771 (*KCNJ15*; B) from non-Asian AD cohorts. Values of effect size (log OR) obtained from independent datasets or metaresults are denoted by rectangles and diamonds, respectively. For the independent dataset, lines indicate the range of 95% confidence intervals, and the sizes of rectangles are proportional to the weights used in the meta-analysis. For the meta-analysis results, the widths of the diamonds cover the range of 95% confidence intervals. ADNI (AD: 515, NC: 339), ADC (AD: 3,946, NC: 1,746), and LOAD (AD: 464, NC: 2,231). *GCH1* rs72713460: RE $P = 1.55E–02$, effect size = 0.1039; *KCNJ15* rs928771: RE $P = 1.19E–01$, effect size = 0.0554. (C and D) Association of *KCNJ15* with age at onset of AD. (C) Survival plot of cumulative dementia-free probabilities in AD subjects from the LOAD cohort stratified by rs928771 genotypes ($P = 0.0057$, Cox proportional hazards model with adjustment for gender and top-5 PCs; HR = 1.1974; $n = 126$, 204, and 125 for rs928771 genotypes TT, TG, and GG, respectively). (D) Dot plot of individual age at AD onset stratified by *KCNJ15* rs928771 genotype. Data are presented as mean ± SEM, *$P < 0.05$, ANCOVA with Bonferroni correction [$n = 126$, 204, and 125; average (SD) onset age of dementia = 73.4 (7.6), 73.0 (6.6), and 71.2 (6.8) for rs928771 genotypes TT, TG, and GG, respectively; $F = 6.35$ for rs928771 genotype TT vs. GG in AD].

Table 2. Replication study of AD susceptibility loci in multiple datasets

Variants	Genes	Cohorts	P value	Effect size	SE	Meta (REs)							
						P value	Log OR (±SD)	OR	I^2	Q	P value (Q)	Tau^2
rs72713460*	GCH1	ADNI	9.60E−02	0.2154	0.1294	1.55E−02	0.1039 (±0.0429)	1.109	0.000	0.987	0.610	0.000
		ADC	1.44E−01	0.0788	0.0539							
		LOAD	1.64E−01	0.1181	0.0849							
rs928771	KCNJ15	ADNI	7.44E−01	0.0338	0.1035	1.19E−01	0.0554 (±0.0356)	1.057	0.000	0.051	0.975	0.000
		ADC	1.93E−01	0.0574	0.0441							
		LOAD	4.11E−01	0.0607	0.0738							
rs2591054	LINC01413	ADNI	5.59E−01	0.0630	0.1077	5.19E−01	−0.0375 (±0.0581)	0.963	50.398	4.032	0.133	0.005
		ADC†	8.27E−03	−0.1167	0.0442							
		LOAD	8.17E−01	0.0170	0.0733							

Three previously published GWAS AD cohorts with clinically diagnosed AD cases and healthy NCs were included into the meta-analysis: ADNI (AD: 515, NC: 339), ADC (AD: 3,946, NC: 1,746), and LOAD (AD: 464, NC: 2,231). Effect size and SE are shown accordingly. Meta-P values were obtained from the METASOFT program on the basis of the estimation of the RE model. I^2, I-square heterogeneity statistic; Q, Cochrane's Q statistic; Tau^2, Tau-square heterogeneity estimator of DerSimonian–Laird.
*Variant(s) with $P < 5E-2/3 = 1.6E-2$ in the meta-analysis results.
†Statistical metrics with $P < 5E-2/3 = 1.6E-2$ in the corresponding cohorts.

The transcript level of *GCH1* was enriched in hematopoietic cells of the myeloid and B lymphoid lineages ($P = 6.67 \times 10^{-59}$, fold-enrichment: 16.9) (Fig. 5A). Moreover, we observed genotype-dependent regulation of *GCH1* transcript level in the caudate nucleus region of the brain (Fig. 5B). These findings suggest that multiple systems or cell types in the brain and blood may be associated with GCH1 signaling. Our analysis of the genotype-dependent regulation of plasma biomarkers in AD patients identified the allele-dependent alterations of matrixmetalloproteinase-2 (MMP-2) in AD subjects (Fig. 5C and *SI Appendix*, Tables S11 and S12).

Regulatory Roles of AD Susceptibility Loci in Immune-Associated Signatures. To investigate the possible disease mechanisms of the identified AD risk loci, we subjected the 52 variants at the three AD risk loci (two from *KCNJ15*, one from *GCH1*, and the remaining from *APOE* and the surrounding region) to a global analysis of genotype–expression associations. Because AD is associated with progressive memory loss and immune functions, as evidenced by the identification of immune genes in Caucasian GWAS (3–8), we specifically examined the possible regulatory effects of the identified AD risk loci in the hippocampus and blood. Primary investigations of genotype–expression associations revealed changes in the monocyte markers (*APOE*-locus for CD68), MHC molecules (*KCNJ15* for HLA-A), and epigenetic modifier (*GCH1* for HDAC1) in the hippocampus (Fig. 6A, *Left*). Meanwhile, for *GCH1*, we observed effects on the regulation of an AD risk gene, clusterin, as well as complement genes (C1QA, C1QB, and C1QC) in blood (Fig. 6A, *Right*). These findings suggest that the identified AD risk loci regulate immune signatures in the central nervous system and peripheral blood.

Furthermore, network analysis revealed enrichment of protein–protein interactions among the genes that showed correlations between their transcript level changes and the identified AD risk variants (P values for protein–protein interactions in the hippocampus and blood: $P = 5.64 \times 10^{-4}$ and 3.14×10^{-4}, respectively) (Fig. 6A). Next, we performed gene ontology (GO) analysis for genes in the network. Interestingly, AD risk loci were strongly associated with changes of the immune-associated gene signatures in both the hippocampus and blood, as evidenced by the enrichment of genes involving in cellular response to cytokine stimulus [false-discovery rate (FDR) = 2.0×10^{-5}] and innate immune response (FDR = 5.6×10^{-4}) in the hippocampal network, as well as defense response (FDR = 3.6×10^{-6}), innate immune response (FDR = 1.3×10^{-5}), and complement

activation (FDR = 2.0×10^{-4}) in the blood network (Fig. 6B, *Right*, and *SI Appendix*, Table S13). These findings suggest that the identified AD risk loci may exert their effects in AD through the regulation of immune-related pathways.

Replication of Caucasian Risk Loci in the Chinese WGS Dataset. We examined the contributions of Caucasian AD GWAS risk variants in the Chinese AD cohort using the existing WGS data (*SI Appendix*, Table S14). To ensure the accuracy of variant detection, among the 21 known risk loci identified in AD meta-analyses (35), we excluded five sites because of their low frequency in the Chinese population (MAF < 5%). Among the remaining 16 sites, based on our current data, only three showed hints of association with AD (*BIN1* rs6733839, adjusted $P = 4.7 \times 10^{-2}$; *CD2AP* rs10948363, adjusted $P = 4.5 \times 10^{-2}$; *FERMT2* rs17125944, adjusted $P = 3.6 \times 10^{-2}$) (*SI Appendix*, Table S14). None of these three variants were located in repetitive regions, indicating good detection quality. Furthermore, concordant risk or protective effects were observed in both the Chinese and Caucasian datasets (Caucasian and Chinese datasets, respectively: *BIN1* rs6733839-T, OR = 1.21 and 1.21; *CD2AP* rs10948363-G, OR = 1.10 and 1.33; *FERMT2* rs17125944-C, OR = 0.76 and 0.79) (*SI Appendix*, Table S14). These findings highlight the role of AD risk variants in multiple ethnic groups and also imply that ethnicity potentially contributes to the genetic basis of AD, as reflected by the observed differences in the population frequencies or disease risk effects for the specific AD risk variants studied herein.

Discussion

In this study, we comprehensively analyzed AD susceptibility loci in WGS data obtained from an AD cohort of Han Chinese ancestry. Our study revealed several common AD genetic risk factors, including *APOE*, *GCH1*, and *KCNJ15*. We revalidated the risk effects of the two identified risk loci, *GCH1* (rs72713460) and *KCNJ15* (rs928771), either by genotype–phenotype association or onset-age analysis in AD cases. Genotype–expression association analysis enables us to investigate the roles of aforementioned AD risk loci by demonstrating their effects on the regulation of genes in the hippocampus and blood. The associations of the identified AD risk loci and changes in the plasma biomarkers suggest that these loci have functional outcomes in the peripheral immune system of AD patients.

APOE is a well-accepted genetic marker for late-onset AD, and the ε4 allele of the *APOE* gene is the strongest genetic risk factor for the disease (51, 52). While previous GWAS show the
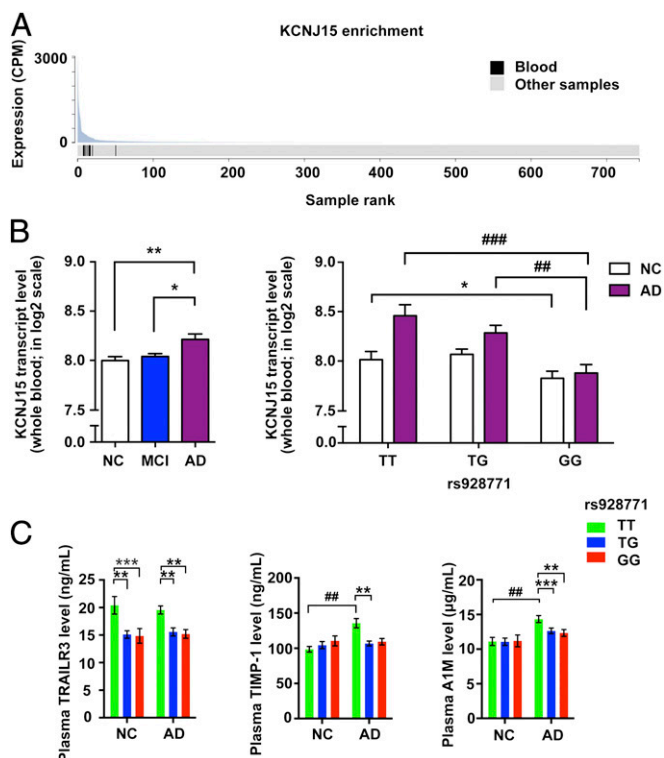
Fig. 4. Functional evidence of *KCNJ15* in AD. (*A*) Among different tissue samples, the *KCNJ15* transcript was most abundant in blood as suggested by the lowest *P* value of enrichment ($P = 6.33E{-}7$, fold-enrichment = 10.6; nine blood samples in 735 total samples). The figure was adopted from the FANTOM CAT database. (*B*) Genotype- and phenotype-dependent regulation of *KCNJ15* transcript level in blood transcriptome data. (*Left*) Increased *KCNJ15* transcript level in the whole blood of AD subjects (NC: 244, MCI: 369, AD: 106). Data are presented as mean ± SEM **$P < 0.01$, *$P < 0.05$, ANCOVA with Bonferroni correction ($F = 10.38$ and 5.93, for AD vs. NC, AD vs. MCI, respectively). (*Right*) The change of KCNJ15 transcript level in whole blood is associated with *KCNJ15* rs928771 genotypes in NC and AD subjects; data are presented as mean ± SEM, *$P < 0.05$ for NC subjects ($n = 77$, 114, and 53 for rs928771 genotypes TT, TG, and GG, respectively; $F = 8.22$, for rs928771 TT vs. GG in NC). ##$P < 0.01$, ###$P < 0.001$ for AD subjects, ANCOVA with Bonferroni correction ($n = 28$, 49, and 29 for rs928771 genotypes TT, TG, and GG, respectively; $F = 13.55$, 10.21 for rs928771 genotypes TT vs. GG, TG vs. GG, respectively). (*C*) Associations between *KCNJ15* rs928771 genotype and biomarker levels in AD cases and NCs. Data are presented as mean ± SEM. Test for genotypes, **$P < 0.01$, ***$P < 0.001$; test for phenotypes, ###$P < 0.001$ (AD: $n = 31$, 46, and 26; NC: $n = 23$, 23, and 11 for rs928771 genotypes TT, TG, and GG, respectively), ANCOVA with Bonferroni correction. cpm, counts per million mapped reads.

existence of multiple AD-risk variants in and around the *APOE* region (53–55), adoption of the WGS method enabled a comprehensive examination of this locus, obtaining fine-mapping results of the variants that are associated with AD risk as well as the magnitude of LD between variants (*SI Appendix*, Tables S5 and S9). A previous fine-mapping study using the Sanger genotyping method conducted in a Japanese AD cohort reported multiple hints and haplotypes in the *APOE* locus that are associated with AD (56). By utilizing the WGS method, we not only obtained a larger AD-risk variant pool including the sentinel variant rs73052335, but also observed a similar AD-associated genomic structure among Chinese and Japanese populations in this region (indicated by the distributions of both *P* values and recombination hot spots) (Fig. 2*B*) (56), demonstrating the advantages of the WGS method in resolving genomic structures in the disease context, and a similar genetic mechanism for AD among Chinese and Japanese for the *APOE* locus.

In our study, *GCH1* and *KCNJ15* were identified as genetic risk loci for AD. *GCH1* encodes the enzyme GTP cyclohydrolase I, which is a rate-limiting enzyme for the biosynthesis of tetrahydrobiopterin (THB, BH4); the protein is critical for the generation of monoamine neurotransmitters such as serotonin (5-HT) and dopamine, as well as nitric oxide. Mutations of *GCH1* are associated with multiple neuronal disorders including dopamine-responsive dystonia (57–59), neuropathic pain (60, 61), and Parkinson's disease (62–64). *GCH1* is also implicated in cardiovascular functions, as suggested by the associations of genetic variants with endophenotypes, including nitric oxide excretion and cardiac autonomic traits (65). The association of *GCH1* rs72713460 with the change in the levels of plasma MMP-2 suggests that *GCH1* may play a role in the immune system or amyloid-β–associated metabolic pathway in addition to modulating neurotransmitter levels (66, 67).

Meanwhile, *KCNJ15* is a member of the potassium voltage-gated channel family and is located in the Down syndrome chromosome region-1; it has been reported to be associated with type 2 diabetes mellitus (T2DM) in the Japanese population (68, 69). *KCNJ15* also plays roles in glucose response, insulin secretion, and blood-related traits (70–72). The effect of sentinel AD risk variant of *KCNJ15*, rs928771, on the age at onset of AD, suggests its potential effect on AD pathogenesis or progression. Interestingly, *KCNJ15* variant rs3746876, the protective variant for T2DM, is in proximity to rs928771 (∼8 kb apart in this study and ref. 69). These two sites are in weak LD ($R^2 = 0.013$, $D' = 1.0$; 1000 Genomes data CHB + JPT), and their minor alleles may be located in separate haplotypes. Haplotype analysis of the *KCNJ15* gene may help to dissect the contributions of *KCNJ15* to AD and T2DM. It would be interesting to examine whether *KCNJ15* exerts its effect on AD or T2DM in East Asians through independent or convergent mechanisms.

The genotype–expression association analysis highlights a role of the *KCN15* variant rs928771 in the modulation of *KCNJ15*
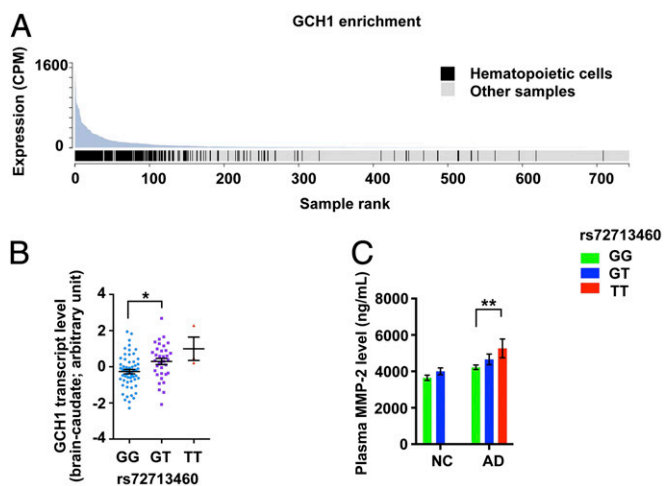

Fig. 5. Functional evidence of *GCH1* in AD. (*A*) GCH1 transcript was most abundant in the hematopoietic cells among all samples as suggested by lowest *P* value of enrichment ($P = 6.67E{-}59$, fold-enrichment = 16.9; 163 hematopoietic cell samples in 581 total samples). The figure was adopted from the FANTOM CAT database. (*B*) Associations between *GCH1* transcript levels and *GCH1* rs72713460 genotypes in the brain caudate region ($n = 57$, 34, and 3 for rs72713460 genotypes GG, GT, and TT, respectively). Data are presented as mean ± SEM, *$P < 0.05$ ($F = 6.58$); ANCOVA with Bonferroni correction. (*C*) *GCH1* rs72713460 genotype is associated with plasma MMP-2 levels. Levels of MMP-2 in AD cases and NCs [AD: $n = 64$, 32, and 7; NC: $n = 37$, 19, and 1 (removed from analysis) for rs72713460 genotypes GG, GT, and TT, respectively]. Data are presented as mean ± SEM **$P < 0.01$ ($F = 8.59$); ANCOVA with Bonferroni correction.
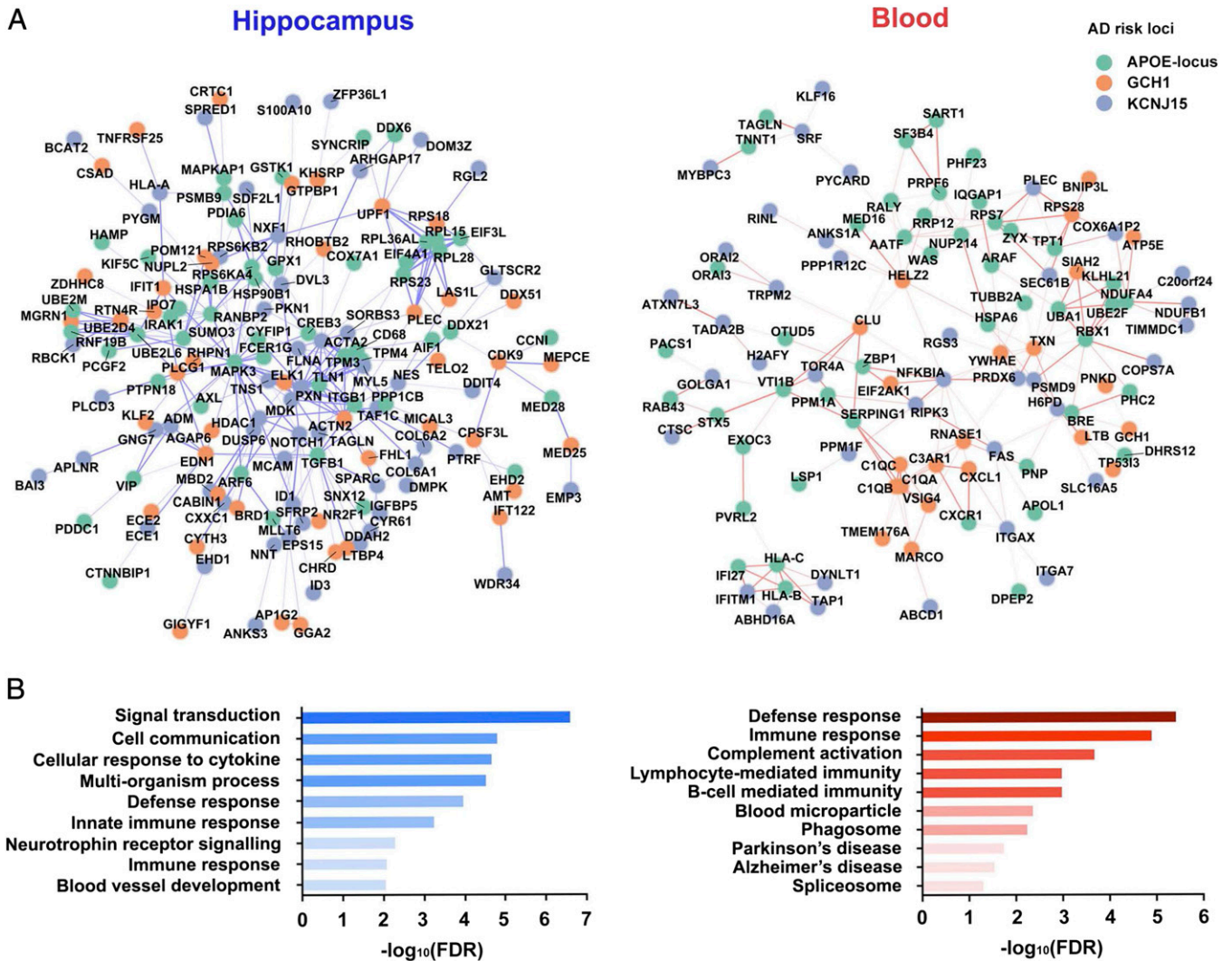
Fig. 6. Enrichment of immune-associated context in the regulatory network of AD risk loci. Association of candidate target genes with AD risk loci by global genotype-expression analysis. (*A*) Interaction network of the target genes regulated by the AD susceptibility loci in the hippocampus (*n* = 87, *Left*) and blood (*n* = 365, *Right*). Each circle represents a target gene, with different colors specifying the corresponding AD risk loci. Lines between circles indicate gene–gene interactions. The strength of the pairwise interaction between the target genes is reflected by the color intensity of the lines. (*B*) GO analysis of the target genes. Representative enriched GO terms for target genes from hippocampal data (*Left*) and blood data (*Right*) are shown; *x* axis indicates the corresponding FDR (in log$_{10}$ scale), with corresponding ontology categories marked on the *y* axis.

transcript level in the blood. Meanwhile, the opposite effect was observed between genotype and phenotype: the *KCNJ15* transcript level was elevated in AD but is down-regulated by the risk G allele of rs928771 in all phenotypic groups (Fig. 4). Because the risk allele G is associated with both advanced onset of AD and lower *KCNJ15* transcript level, and because the *KCNJ15* transcript level is positively associated with individual cognitive performance (Figs. 3 and 4 and *SI Appendix*, Fig. S5), *KCNJ15* expression in the blood may confer a protective effect during AD progression. Specifically, the plasma biomarker analysis in AD subjects revealed the modulatory effects of rs928771 in inflammation (i.e., A1M) (Fig. 4), Aβ metabolism (modulation of ADAM10 activity by TIMP-1) (73), and cell homeostasis (TRAILR3 and TIMP-1) (74, 75). Therefore, it is of interest to study the effect of *KCNJ15* variants in inflammatory response, which may contribute to the pathogenesis of AD.

Our transcriptome and biomarker studies suggest that *GCH1* and *KCNJ15* are highly expressed in the immune system and are involved in immune-related events. This is congruent with previous findings showing an etiological role of the immune system

on AD, including the identification of rare *TREM2* variants (3, 4), risk genes marked by the common variants from Caucasian GWAS (7, 35), and the latest report for rare coding variants in *PLCG2* and *ABI3* identified from Caucasian AD patients (8). Modulations of immune signatures or biomarker levels in blood led by identified AD risk variant, as well as enriched expression of *GCH1* and *KCNJ15* in the blood or blood cells, further supports the roles of immune pathways, specifically in the peripheral circulatory system, in AD. Interestingly, previous studies show that alterations of genetic signatures in the peripheral circulatory system are associated with several brain disorders, including autism (76), Parkinson's disease (77), and schizophrenia (78). Thus, comprehensive profiling of peripheral biomarkers in AD patients, including transcript, protein, or metabolite levels, may benefit the prediction and monitoring of AD.

In conclusion, we successfully implemented the low-pass WGS method to identify two AD susceptibility loci represented by common disease-associated variants in the Chinese population. Moreover, genotype–expression association analysis suggests that the identification of the genetic variants may not only

1. Chan KY, et al.; Global Health Epidemiology Reference Group (GHERG) (2013) Epidemiology of Alzheimer's disease and other forms of dementia in China, 1990-2010: A systematic review and analysis. *Lancet* 381:2016–2023.
2. Guerreiro R, Hardy J (2014) Genetics of Alzheimer's disease. *Neurotherapeutics* 11:732–737.
3. Guerreiro R, et al.; Alzheimer Genetic Analysis Group (2013) TREM2 variants in Alzheimer's disease. *N Engl J Med* 368:117–127.
4. Jonsson T, et al. (2013) Variant of TREM2 associated with the risk of Alzheimer's disease. *N Engl J Med* 368:107–116.
5. Griciuc A, et al. (2013) Alzheimer's disease risk gene CD33 inhibits microglial uptake of amyloid beta. *Neuron* 78:631–643.
6. Wang Y, et al. (2015) TREM2 lipid sensing sustains the microglial response in an Alzheimer's disease model. *Cell* 160:1061–1071.
7. Huang KL, et al.; International Genomics of Alzheimer's Project; Alzheimer's Disease Neuroimaging Initiative (2017) A common haplotype lowers PU.1 expression in myeloid cells and delays onset of Alzheimer's disease. *Nat Neurosci* 20:1052–1061.
8. Sims R, et al.; ARUK Consortium; GERAD/PERADES, CHARGE, ADGC, EADI (2017) Rare coding variants in PLCG2, ABI3, and TREM2 implicate microglial-mediated innate immunity in Alzheimer's disease. *Nat Genet* 49:1373–1384.
9. Gilligan AM, Malone DC, Warholak TL, Armstrong EP (2012) Racial and ethnic disparities in Alzheimer's disease pharmacotherapy exposure: An analysis across four state Medicaid populations. *Am J Geriatr Pharmacother* 10:303–312.
10. Hallman DM, et al. (1991) The apolipoprotein E polymorphism: A comparison of allele frequencies and effects in nine populations. *Am J Hum Genet* 49:338–349.
11. Wang HZ, et al. (2016) Validating GWAS-identified risk loci for Alzheimer's disease in Han Chinese populations. *Mol Neurobiol* 53:379–390.
12. Guo JF, et al. (2015) Polygenic determinants of Parkinson's disease in a Chinese population. *Neurobiol Aging* 36:1765.e1–1765.e6.
13. Huang Y, et al. (2015) SNCA gene, but not MAPT, influences onset age of Parkinson's disease in Chinese and Australians. *BioMed Res Int* 2015:135674.
14. Huang M, et al. (2015) Lack of genetic association between TREM2 and Alzheimer's disease in East Asian population: A systematic review and meta-analysis. *Am J Alzheimers Dis Other Demen* 30:541–546.
15. Ma J, et al. (2014) Association study of TREM2 polymorphism rs75932628 with late-onset Alzheimer's disease in Chinese Han population. *Neurol Res* 36:894–896.
16. Miyashita A, et al. (2014) Lack of genetic association between TREM2 and late-onset Alzheimer's disease in a Japanese population. *J Alzheimers Dis* 41:1031–1038.
17. Jiang T, et al. (2016) A rare coding variant in TREM2 increases risk for Alzheimer's disease in Han Chinese. *Neurobiol Aging* 42:217.e1–3.
18. Xiao X, Chang H, Li M (2017) Molecular mechanisms underlying noncoding risk variations in psychiatric genetic studies. *Mol Psychiatry* 22:497–511.
19. Cruchaga C, et al.; GERAD Consortium; Alzheimer's Disease Neuroimaging Initiative (ADNI); Alzheimer Disease Genetic Consortium (ADGC) (2013) GWAS of cerebrospinal fluid tau levels identifies risk variants for Alzheimer's disease. *Neuron* 78:256–268.
20. Ramanan VK, et al.; Alzheimer's Disease Neuroimaging Initiative (ADNI) (2015) GWAS of longitudinal amyloid accumulation on 18F-florbetapir PET in Alzheimer's disease implicates microglial activation gene IL1RAP. *Brain* 138:3076–3088.
21. Shen L, et al.; Alzheimer's Disease Neuroimaging Initiative (2010) Whole genome association study of brain-wide imaging phenotypes for identifying quantitative trait loci in MCI and AD: A study of the ADNI cohort. *Neuroimage* 53:1051–1063.
22. Zhu Z, et al. (2016) Integration of summary data from GWAS and eQTL studies predicts complex trait gene targets. *Nat Genet* 48:481–487.
23. McKhann GM, et al. (2011) The diagnosis of dementia due to Alzheimer's disease: Recommendations from the National Institute on Aging-Alzheimer's Association workgroups on diagnostic guidelines for Alzheimer's disease. *Alzheimers Dement* 7:263–269.
24. Petersen RC (2004) Mild cognitive impairment as a diagnostic entity. *J Intern Med* 256:183–194.
25. Cai N, et al. (2017) Data descriptor: 11,670 whole-genome sequences representative of the Han Chinese population from the CONVERGE project. *Sci Data* 4:170011.
26. Jun G, Wing MK, Abecasis GR, Kang HM (2015) An efficient and scalable analysis framework for variant extraction and refinement from population-scale DNA sequence data. *Genome Res* 25:918–925.
27. Andrews S (2014) FastQC: A quality control tool for high throughput sequence data. Version 0.11.2. Available at www.bioinformatics.babraham.ac.uk/projects/fastqc/. Accessed August 12, 2015.
28. Bolger AM, Lohse M, Usadel B (2014) Trimmomatic: A flexible trimmer for Illumina sequence data. *Bioinformatics* 30:2114–2120.
29. Browning SR, Browning BL (2007) Rapid and accurate haplotype phasing and missing-data inference for whole-genome association studies by use of localized haplotype clustering. *Am J Hum Genet* 81:1084–1097.
30. Browning BL, Browning SR (2009) A unified approach to genotype imputation and haplotype-phase inference for large data sets of trios and unrelated individuals. *Am J Hum Genet* 84:210–223.
31. CRAN (2017) R (Short summer). Version 3.4.2. Available at https://www.r-project.org/. Accessed November 2, 2017.
32. Guan W, Liang L, Boehnke M, Abecasis GR (2009) Genotype-based matching to correct for population stratification in large-scale case-control genetic association studies. *Genet Epidemiol* 33:508–517.
33. Price AL, et al. (2006) Principal components analysis corrects for stratification in genome-wide association studies. *Nat Genet* 38:904–909.

34. Pruim RJ, et al. (2010) LocusZoom: Regional visualization of genome-wide association scan results. *Bioinformatics* 26:2336–2337.

35. Lambert JC, et al.; European Alzheimer's Disease Initiative (EADI); Genetic and Environmental Risk in Alzheimer's Disease; Alzheimer's Disease Genetic Consortium; Cohorts for Heart and Aging Research in Genomic Epidemiology (2013) Meta-analysis of 74,046 individuals identifies 11 new susceptibility loci for Alzheimer's disease. *Nat Genet* 45:1452–1458.

36. Weiner MW, et al. (2010) The Alzheimer's disease neuroimaging initiative: Progress report and future plans. *Alzheimers Dement* 6:202.e7–211.e7.

37. Morris JC, et al. (2006) The Uniform Data Set (UDS): Clinical and cognitive variables and descriptive data from Alzheimer disease centers. *Alzheimer Dis Assoc Disord* 20: 210–216.

38. Lee JH, Cheng R, Graff-Radford N, Foroud T, Mayeux R; National Institute on Aging Late-Onset Alzheimer's Disease Family Study Group (2008) Analyses of the National Institute on Aging Late-Onset Alzheimer's Disease family study: Implication of additional loci. *Arch Neurol* 65:1518–1526.

39. Han B, Eskin E (2011) Random-effects model aimed at discovering associations in meta-analysis of genome-wide association studies. *Am J Hum Genet* 88:586–598.

40. Kang EY, et al. (2016) ForestPMPlot: A flexible tool for visualizing heterogeneity between studies in meta-analysis. *G3 (Bethesda)* 6:1793–1798.

41. Consortium GT; GTEx Consortium (2015) Human genomics. The genotype-tissue expression (GTEx) pilot analysis: Multitissue gene regulation in humans. *Science* 348: 648–660.

42. Carithers LJ, et al.; GTEx Consortium (2015) A novel approach to high-quality postmortem tissue procurement: The GTEx project. *Biopreserv Biobank* 13:311–319.

43. Karssen L, Team G (2013) New software and developments in the GenABEL project. *Hum Hered* 76:111.

44. Szklarczyk D, et al. (2015) STRING v10: Protein-protein interaction networks, integrated over the tree of life. *Nucleic Acids Res* 43:D447–D452.

45. Basham B (1997) Graphpad prism. *Biotechnol Softw J* 14:14–17.

46. Kent WJ, et al. (2002) The human genome browser at UCSC. *Genome Res* 12: 996–1006.

47. Hon CC, et al. (2017) An atlas of human long non-coding RNAs with accurate 5′ ends. *Nature* 543:199–204.

48. Gauderman W, Morrison J (2009) QUANTO 1.1: A computer program for power and sample size calculations for genetic-epidemiology studies. Available at biostats.usc.edu/Quanto.html. Accessed April 25, 2017.

49. Li Y, Sidore C, Kang HM, Boehnke M, Abecasis GR (2011) Low-coverage sequencing: Implications for design of complex trait association studies. *Genome Res* 21:940–951.

50. Epstein MP, et al. (2012) Stratification-score matching improves correction for confounding by population stratification in case-control association studies. *Genet Epidemiol* 36:195–205.

51. Corder EH, et al. (1993) Gene dose of apolipoprotein E type 4 allele and the risk of Alzheimer's disease in late onset families. *Science* 261:921–923.

52. Genin E, et al. (2011) APOE and Alzheimer disease: A major gene with semi-dominant inheritance. *Mol Psychiatry* 16:903–907.

53. Helisalmi S, et al. (1999) Promoter polymorphism (-491A/T) in the APOE gene of Finnish Alzheimer's disease patients and control individuals. *J Neurol* 246:821–824.

54. Roses AD, et al. (2010) A TOMM40 variable-length polymorphism predicts the age of late-onset Alzheimer's disease. *Pharmacogenomics J* 10:375–384.

55. Carrasquillo MM, Morgan K (2012) Commentary on 'Functional analysis of APOE locus genetic variation implicates regional enhancers in the regulation of both TOMM40 and APOE'. *J Hum Genet* 57:3–4.

56. Takei N, et al.; Japanese Genetic Study Consortium for Alzheimer Disease (2009) Genetic association study on in and around the APOE in late-onset Alzheimer disease in Japanese. *Genomics* 93:441–448.

57. Steinberger D, et al. (1998) High penetrance and pronounced variation in expressivity of GCH1 mutations in five families with dopa-responsive dystonia. *Ann Neurol* 43: 634–639.

58. Steinberger D, et al.; German Dystonia Study Group (2000) Dopa-responsive dystonia: Mutation analysis of GCH1 and analysis of therapeutic doses of L-dopa. *Neurology* 55: 1735–1737.

59. Shi WT, Cai CY, Li MS, Ling C, Li WD (2015) Han Chinese patients with dopa-responsive dystonia exhibit a low frequency of exonic deletion in the GCH1 gene. *Genet Mol Res* 14:11185–11190.

60. Taylor JG, et al. (2009) A GCH1 haplotype associated with susceptibility to vaso-occlusive pain and impaired vascular function in sickle cell anemia. *Blood* 114:575.

61. Belfer I, et al. (2014) A GCH1 haplotype confers sex-specific susceptibility to pain crises and altered endothelial function in adults with sickle cell anemia. *Am J Hematol* 89: 187–193.

62. Cobb SA, et al. (2009) GCH1 in early-onset Parkinson's disease. *Mov Disord* 24: 2070–2075.

63. Webb J, Willette AA (2017) Aging modifies the effect of GCH1 RS11158026 on DAT uptake and Parkinson's disease clinical severity. *Neurobiol Aging* 50:39–46.

64. Mencacci NE, et al.; International Parkinson's Disease Genomics Consortium and UCL-exomes consortium (2014) Parkinson's disease in GTP cyclohydrolase 1 mutation carriers. *Brain* 137:2480–2492.

65. Zhang L, et al. (2007) Discovery of common human genetic variants of GTP cyclohydrolase 1 (GCH1) governing nitric oxide, autonomic activity, and cardiovascular risk. *J Clin Invest* 117:2658–2671.

66. Yin KJ, et al. (2006) Matrix metalloproteinases expressed by astrocytes mediate extracellular amyloid-beta peptide catabolism. *J Neurosci* 26:10939–10948.

67. Detry B, et al. (2012) Matrix metalloproteinase-2 governs lymphatic vessel formation as an interstitial collagenase. *Blood* 119:5048–5056.

68. Okamoto K, et al. (2010) Identification of KCNJ15 as a susceptibility gene in Asian patients with type 2 diabetes mellitus. *Am J Hum Genet* 86:54–64.

69. Fukuda H, et al. (2013) Replication study for the association of a single-nucleotide polymorphism, rs3746876, within KCNJ15, with susceptibility to type 2 diabetes in a Japanese population. *J Hum Genet* 58:490–493.

70. Gosset P, et al. (1997) A new inward rectifier potassium channel gene (KCNJ15) localized on chromosome 21 in the Down syndrome chromosome region 1 (DCR1). *Genomics* 44:237–241.

71. Okamoto K, et al. (2012) Inhibition of glucose-stimulated insulin secretion by KCNJ15, a newly identified susceptibility gene for type 2 diabetes. *Diabetes* 61:1734–1741.

72. Lee JB, Yoo CK, Park HB, Cho IC, Lim HT (2016) Association of the single nucleotide polymorphisms in RUNX1, DYRK1A, and KCNJ15 with blood related traits in pigs. *Asian-Australas J Anim Sci* 29:1675–1681.

73. Amour A, et al. (2000) The in vitro activity of ADAM-10 is inhibited by TIMP-1 and TIMP-3. *FEBS Lett* 473:275–279.

74. Sheridan JP, et al. (1997) Control of TRAIL-induced apoptosis by a family of signaling and decoy receptors. *Science* 277:818–821.

75. Rho SB, Chung BM, Lee JH (2007) TIMP-1 regulates cell proliferation by interacting with the ninth zinc finger domain of PLZF. *J Cell Biochem* 101:57–67.

76. Ashwood P, Wakefield AJ (2006) Immune activation of peripheral blood and mucosal CD3+ lymphocyte cytokine profiles in children with autism and gastrointestinal symptoms. *J Neuroimmunol* 173:126–134.

77. Masliah E, Dumaop W, Galasko D, Desplats P (2013) Distinctive patterns of DNA methylation associated with Parkinson disease: Identification of concordant epigenetic changes in brain and peripheral blood leukocytes. *Epigenetics* 8:1030–1038.

78. Bowden NA, et al. (2006) Preliminary investigation of gene expression profiles in peripheral blood lymphocytes in schizophrenia. *Schizophr Res* 82:175–183.